

ARTICLE

Open Access

Naked-eye point-of-care testing platform based on a pH-responsive superwetting surface: toward the non-invasive detection of glucose

Zhong Feng Gao¹, Ei Ei Sann¹, Xiaoding Lou^{1,2}, Renyi Liu², Jun Dai¹, Xiaolei Zuo³, Fan Xia^{1,2} and Lei Jiang⁴

Abstract

Herein, we demonstrate a contact angle (CA)-based naked-eye point-of-care testing platform with rapid pH-responsive superwettability that can switch between superhydrophilic and superhydrophobic properties for quantitative biosensing. The CA of the droplet on the pH-responsive surface approached $\sim 0^\circ$ at pH 1 and conversely reached $161.4^\circ \pm 6.2^\circ$ at pH 13. We realized the sensitive detection of the pH, urea, and glucose by monitoring the changes in the CA. The traditional invasive diagnosis of diabetes causes pain and brings the risk of infections, such as acquired immune deficiency syndrome (AIDS), hepatitis B, hepatitis C, and syphilis, to the user. To address this issue, we implemented a method for the non-invasive diagnosis of diabetes in human saliva and urine, which avoided the significant drawbacks mentioned above. The accuracy of this method was demonstrated by comparing the results with those from commercial glucometers and theoretical calculations. Interestingly, we successfully monitored glucose levels in sweat before, during, and after cycling. The sensing performance was barely influenced by the temperature, elevation, and droplet color, illustrating promise for expansion to hundreds of millions of potential customers, especially those with color blindness or color weakness. Given its low cost, lack of instruments, and rapid response (within 1 s), this strategy might overcome the limitations of the mechanical stability and durability of superwetable materials and thus might extend the industrial-scale application of bioinspired superwetable systems.

Introduction

Learning from nature provides an exciting strategy for constructing smart and functional materials. In nature, many biological materials display significant stimuli-responsive surface wettability¹. For instance, the leaves of *Pinus sylvestris* treated with gaseous air pollutants

exhibited an increase in the contact angle (CA)². The leaves of *Phaseolus vulgaris* L., *Pisum sativum* L., *Vicia faba* L., and *Brassica napus* L. became less hydrophilic following exposure to acid rain³. Stimuli-responsive materials, which are functionally similar in wettability to natural surfaces, have been developed for bioseparation⁴, drug delivery systems^{5,6}, cell-based diagnostics⁷, biosensing^{8,9}, and so on^{10,11}. By combining stimuli-responsive materials with microstructures or nanostructures, smart switching between superhydrophobic and superhydrophilic properties has been realized in the last two decades^{12–14}. The current applications of superwetable materials, such as self-cleaning¹⁵, anti-icing¹⁶, water harvesting¹⁷, printing¹⁸, and water–oil separation¹⁹, are generally restricted to the industrial field because they

Correspondence: Jun Dai (dj_hust1987@sina.com) or Fan Xia (xiafan@cug.edu.cn)

¹Hubei Key Laboratory of Bioinorganic Chemistry & Materia Medica, School of Chemistry and Chemical Engineering, Department of Obstetrics and Gynecology, Tongji Hospital, Tongji Medical College, Huazhong University of Science and Technology, 430074 Wuhan, China

²Engineering Research Center of Nano-Geomaterials of Ministry of Education, Faculty of Materials Science and Chemistry, China University of Geosciences, 388 Lumo Road, 430074 Wuhan, China

Full list of author information is available at the end of the article

These authors contributed equally: Zhong Feng Gao, Ei Ei Sann, Xiaoding Lou.

© The Author(s) 2018



Open Access This article is licensed under a Creative Commons Attribution 4.0 International License, which permits use, sharing, adaptation, distribution and reproduction in any medium or format, as long as you give appropriate credit to the original author(s) and the source, provide a link to the Creative Commons license, and indicate if changes were made. The images or other third party material in this article are included in the article's Creative Commons license, unless indicated otherwise in a credit line to the material. If material is not included in the article's Creative Commons license and your intended use is not permitted by statutory regulation or exceeds the permitted use, you will need to obtain permission directly from the copyright holder. To view a copy of this license, visit <http://creativecommons.org/licenses/by/4.0/>.

need long-term operation processes, which might enhance the likelihood of damaging the functional surface by external forces¹. To address this challenge, complex structures, chemistries, and materials are being examined worldwide. However, a simple alternative idea is to explore a facile application that needs short-term operation and is not influenced by the mechanical stability and durability of the surface.

Point-of-care testing (POCT) is a rapid diagnostic testing method that satisfies the requirements of the ASSURED (affordable, sensitive, specific, user-friendly, robust, equipment-free, and deliverable to end-users) standard proposed by the World Health Organization²⁰. Significant efforts have been devoted to the development of rapid quantitative readouts in POCT assays, such as optical detection^{21–25}, electrochemical detection^{26–29}, and commercial portable instrument-based detection^{30–33}. While these methods are sensitive and user-friendly, most of them are unsuitable for application with the broad population. Hundreds of millions of people have vision problems worldwide. Color blindness, for instance, affects as many as 8% of men and 0.5% of women³⁴. Thus, optical detection methods, typically those including a lateral flow strip and colorimetric, fluorescence, and chemiluminescence strategies, are not appropriate for people with color blindness or color weakness. Electrochemical detection methods need external equipment, which adds to the complexity and cost of the devices. Commercial portable instruments, such as portable glucometers, ATP meters, pressure meters, and smart phones, increase the testing cost, making them unaffordable in rural and remote areas. Moreover, the customer might experience pain and a risk of infections, such as acquired immune deficiency syndrome (AIDS), hepatitis B, hepatitis C, and syphilis, by using the invasive glucometer. In addition, most of the reported methods focus on single target detection, which cannot satisfy the demands of multiple target detection in complex environments. It is, therefore, desirable to design a generally available, simple, and low-cost POCT platform for multiple target detection.

Since the CA can be simply and visually monitored for wettability characterization, it can be determined by nearly all people, excluding the blind, and thus provides an attractive possibility for utilization in an efficient POCT device. In this study, we developed a naked-eye POCT platform based on the rapid pH⁻ responsive superwettability switch between superhydrophobicity and superhydrophilicity for the detection of pH, urea, and glucose. To control the surface wettability, this pH-responsive superwetting surface consisted of fumed silica nanoparticles that were coated with the organosilanes (3-[2-(2-amino ethylamino) ethylamino] propyl trimethoxy silane (AEPTMS) and octyl trimethoxy silane (OTMS)). Based on the remarkable switch in the wettability, we

achieved the detection of glucose by reading the CA change. The CA decreased with increasing concentration of glucose because the gluconic acid produced from the glucose oxidase-catalyzed reaction led to a decrease in the solution pH. It was demonstrated that a decrease in the CA of human specimens from hydrophobic to hydrophilic by naked-eye detection indicates the occurrence of diabetes. Although other bioinspired materials, for example, nanopores and nanotubes^{35,36}, have been developed for glucose detection, the superwetting surface provides several extraordinary advantages. First, we found that the wettability was barely affected by the ambient temperature and pressure, indicating the wide applicability of this method in all countries. Second, the color of the droplet had no effect on the CA, thereby providing promise for expansion to hundreds of millions of potential customers, especially those that are color-blind or color-weak. Moreover, the low cost, instrument-free, and disposable biosensor presented a rapid sensing response (within 1 s), which avoided long-term operation. Thus, the mechanical stability and durability of the superwettable materials are not crucial factors in biosensing applications. The results are significant for the design and creation of superwettable biosensors and for overcoming the limitations caused by the service life of superwettable materials in practical applications and thus might extend the industrial-scale application of bioinspired superwettable systems.

Experimental section

Materials and instrumentation

AEPTMS and glucose oxidase (GOx) were purchased from Sigma-Aldrich Co. Ltd. (Milwaukee, WI, USA). OTMS was purchased from Xiya Reagent Co. Ltd. (Chengdu, China). Fumed silica nanoparticles (SiNPs) (15, 50, and 200 nm) were purchased from Macklin Biochemical Co., Ltd. (Shanghai, China). Glucose, fructose, galactose, mannose, arabinose, xylose, and ascorbic acid were obtained from Aladdin Chemistry Co., Ltd. (Shanghai, China). Urease was purchased from Worthington Co., Ltd. (Shanghai, China). Urea, glycine, toluene, ethanol, tetrahydrofuran (THF), and other solvents were purchased from Sinopharm Chemical Reagent Co., Ltd. (Beijing, China). All of the chemicals and enzymes used were of analytical grade, and the water used throughout the experiments was Milli-Q ultrapure water. Specimens, including blood, urine and saliva, from normal people and patients with diabetes were obtained from Union Hospital, Tongji Medical College, Huazhong University of Science and Technology. Britton-Robinson buffer was used to prepare solutions with different pH values. An Accu-Chek glucometer was purchased from Roche Company (Ireland), an Contour Plus glucometer was purchased from Bayer Consumer Care AG

(Switzerland), and a OneTouch glucometer was purchased from Johnson and Johnson (USA). The CA was measured using a 2 μL droplet by the OCA20 instrument (DataPhysics, Germany). The surface morphology was characterized by scanning electron microscopy (SEM) using a Hitachi S4800 electron microscope (Japan) at 3.0 kV. X-ray photoelectron spectroscopy (XPS) was performed by using the Thermo ESCALAB 250XI system (USA). Zeta potentials were obtained using the Zetasizer Nano system (UK).

Preparation of pH-responsive silica nanoparticles (pH-SiNPs)

A mixture of SiNPs with different sizes (15, 50, and 200 nm) was heated in an oven at 100 °C for 4 h to remove the moisture. The mixture of SiNPs was placed in a reflux apparatus containing dry toluene, and 1.5 mM solutions containing different ratios of AEPTMS and OTMS were added into it and heated to 110 °C under an inert atmosphere for approximately 4 h. After the reaction was completed, these pH-SiNPs were centrifuged and washed three times with dry toluene to remove the free organosilanes before drying under vacuum at 80 °C.

Preparation of pH-responsive superwetting surfaces

Glass plates were immersed in a hydrogen peroxide solution (30%, H_2O_2) for 3 h to remove dirt and grease. Then, ultrasonication of these glasses was carried out with absolute ethanol for 30 min before thoroughly washing them with plenty of Milli-Q ultrapure water. After that, these glasses were placed in an oven and dried for 1 h at 80 °C. In the coating process, the coating solution was prepared by adding the dried powdered pH-SiNPs into dry THF and stirring the mixture thoroughly for approximately 1 h at room temperature. Then, sonication was performed for another hour. It was better to use this mixture solution immediately while it was fresh. The pH-SiNPs were grafted through self-assembly on the ultraclean glasses by dipping at a rate of 1 mm/s. Before drying in the oven, the glasses were left to stand for approximately 10 min to finish the self-assembly process. After heating at 80 °C for 2 h, the plates were slowly cooled to room temperature before use.

Urea detection using the pH-responsive superwetting surface

For urea detection, we used urea solutions with different concentrations and a 10 U mL^{-1} urease solution. Urea solutions with concentrations ranging from 100 to 3 mM were reacted with the urease solution in phosphate buffer (pH 3) at 37 °C for 10 min. After the reaction was completed, urea detection was accomplished by detection of the generated hydroxyl ions with our as-prepared superwetting surface.

Glucose detection using the pH-responsive superwetting surface

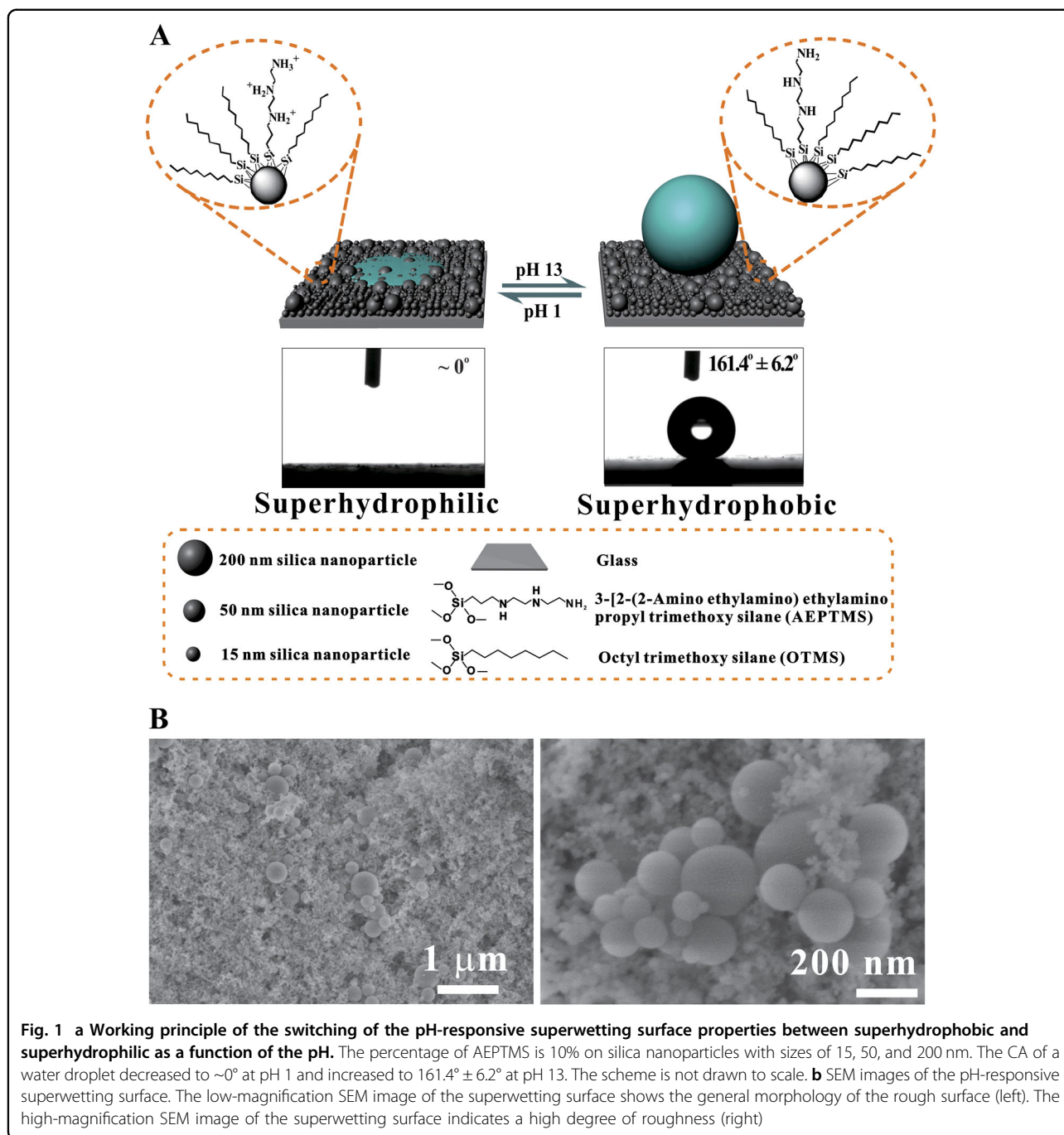
Different concentrations of glucose and GOx were added into PBS (pH 6), which is the optimized condition for GOx. To optimize the incubation time, the reaction was incubated from 0 to 120 min at 37 °C. To optimize the concentration of GOx, the reaction was examined with different GOx concentrations ranging from 1 to 20 U mL^{-1} at 37 °C. The sensitivity test was investigated with the total concentration of glucose ranging from 1 mM to 1 nM with 10 U mL^{-1} GOx at 37 °C for 60 min. For the selectivity test, glucose, fructose, galactose, mannose, arabinose, xylose (total concentration 0.5 mM), and GOx (10 U mL^{-1}) were used for the reaction.

Glucose detection in human blood, urine, saliva and sweat

To evaluate glucose detection in a practical setting, human blood specimens were collected from the 9 patients with diabetes and 9 normal people, and urine and saliva specimens were collected from 9 patients with diabetes and 6 normal people. The blood was collected approximately 2 h after a meal, and the urine and saliva were collected in the early morning. The blood specimens were centrifuged and then diluted 1000 times with a 20 mM PBS buffer solution (pH 7.4) to adjust the glucose concentration into the linear range. The urine specimens were centrifuged and diluted 250 times before use. In addition, the saliva was diluted five times with PBS before use. The glucose oxidase-catalyzed reactions for all specimens were carried out at 37 °C for 60 min. The sweat specimens were gathered from the forehead, breast and back at three times before, during and after student volunteers performed cycling exercise. The sweat was centrifuged and diluted five times with PBS. The detection of glucose in these collected sweat samples was carried out according to the abovementioned procedures.

Results and discussion

To construct the superwetting surface, silica nanoparticles with different sizes (15, 50, and 200 nm) were used to modify the surface topography (Figure S1), promoting the roughness of hierarchical superwetting surfaces¹⁴. The organosilanes hydrophilic AEPTMS and hydrophobic OTMS were employed to functionalize the silica nanoparticles and switch the wettability as a function of the pH (Fig. 1a). The morphology of the as-prepared hierarchical superwetting surface was characterized by scanning electron microscopy (SEM). Different sizes of silica nanoparticles were observed on the rough surface (Fig. 1b). The various sized nanoparticles enhanced the degree of roughness and improved the wettability of the superwetting surface because a large amount of air could be trapped between the droplet and the voids of the surface^{37,38}. Such a high degree of



roughness promoted the liquid repellency, transforming the hydrophobic surface to superhydrophobic or hydrophilic to superhydrophilic¹. X-ray photoelectron spectroscopy (XPS) characterization was further performed to investigate the composition of the as-prepared pH-responsive silica nanoparticles (pH-SiNPs). The spectra of each of the elements Si, C, N, and O were clearly observed with their corresponding binding energies (Figure S2). The C1 s spectrum in the binding energy range of 284.5–285.0 eV revealed the presence of C–C and C–H

groups on the pH–SiNP surfaces. The binding energy of 286.0 eV represented C–N bonds. The C–NH₂ group was observed at a binding energy of approximately 399.2 eV in the N1 s spectrum. The highest peak at a binding energy of 532.0 eV corresponding to the O1 s peak illustrated the presence of abundant Si–O–Si group formed by the reaction of the organosilanes with the silica nanoparticles. A peak at approximately 103.6 eV, which is the Si2 p peak of SiO₂, showed that there was little bare space on the silica nanoparticles^{14,39}. These facts demonstrated that

organosilanes were successfully grafted on the surface of the silica nanoparticles.

As shown in Fig. 1a, AEPTMS and OTMS were important ingredients for achieving the pH response. AEPTMS has hydrophilic properties in acidic solutions due to the protonation of the pH-sensitive amino groups, and OTMS possesses superhydrophobic properties^{14,39}. In the presence of a solution with a pH of 1, the surface was completely wetted within 1 s, and the CA was approximately 0° owing to the protonation of AEPTMS (Figure S3A and Movie S1). When an alkaline solution (pH 13) was dropped on the surface, the amino group of AEPTMS was unprotonated, showing a high CA of 161.4° ± 6.2° with superhydrophobic properties. Thus, the droplet rapidly rolled along the surface at a low rolling angle of 3° (Figure S3B and Movie S1).

Therefore, the use of AEPTMS and OTMS caused the surface properties to switch between superhydrophobic and superhydrophilic as a function of the pH. The response speed of the POCT surface was then studied. It was found that the CA took approximately only 1 s to settle when a droplet with a pH of 1 was dropped on the surface (Fig. 2a). Similarly, Fig. 2b shows that the surface had a rapid response (within 1 s) to the alkaline solution (pH 13). The results reveal the feasibility of the design and creation of a rapid-response superwetable POCT platform.

Zeta potential measurements were conducted to examine the charge of the pH-SiNPs (Figure S4). The measurements revealed that the zeta potential values at pH 5 and pH 7 were positive, which meant that negative ions could approach the positive ions on the surface of the pH-SiNPs because of the protonation of the amino groups on the pH-SiNPs³⁹. However, the zeta potential value decreased to nearly -28 mV at pH 9, indicating that few negative ions attached to the surface of the pH-SiNPs³⁹. Therefore, it was deduced that AEPTMS and OTMS contributed to the hydrophilicity and hydrophobicity of the system and that the rough surface contributed to the creation of superhydrophilicity and superhydrophobicity.

The pH-responsive superwettability was strongly dependent upon the percentage of AEPTMS functional groups on the silica nanoparticles. To achieve the best pH-responsive performance, we prepared various surfaces by changing the percentage of AEPTMS on the silica nanoparticle (0, 10, 50, 90, and 100%), and the wettability was studied as a function of the pH (Figure S5). The absence of AEPTMS caused the surface to be superhydrophobic (CA ≥ 150°) for droplets from pH 1 to 13 because of the lack of amino groups. In the construction of the surface using 10% AEPTMS, the CA linearly increased with increasing the pH from 1 to 7, indicating the remarkable pH-responsive superwettability. As the percentage of AEPTMS further increased, the

performance became unsatisfactory. When the percentage of AEPTMS was above 90%, the surface displayed a strongly superhydrophilic property (CA nearly 0°) due to numerous amino groups of AEPTMS present. Thus, 10% AEPTMS was chosen to prepare the pH-responsive superwetting surface.

To examine the pH-sensitive superwettability of the superwetting surfaces, we investigated the change in the CA with solutions having different pH values using the constructed superwetting surface (Fig. 2c). It can be seen that the CA gradually increased from 0° to 152.5° ± 6.9° with the increase in the pH from 1 to 7. Then, the CA remained nearly constant at 150° and formed a plateau under alkaline conditions, showing the significant superhydrophobicity of the surface. The change in the CA was linear in the pH range of 1 to 7. The linear equation was $y = 25.39x - 25.43$ with a correlation coefficient of 0.986 (Fig. 2d). Figure 2e illustrates visual images of the CA for solutions with different pH values, indicating that the pH can be detected by the naked eye.

To clearly demonstrate the pH response, in situ neutralization was performed on the superwetting surface. The CA of a pH 6 droplet decreased gradually from 126° ± 3.8° to 90° ± 1.9° following the addition of 1 μL of a pH 3 solution (Fig. 2f and Movie S2). After another 1 μL of a pH 1 solution was added, the droplet nearly spread on the surface with a low CA of 30° ± 2.0°. However, the CA changed only slightly in a control test that used a pH 6 solution instead of the pH 3 and pH 1 solutions (Fig. 2g and Movie S2). The in situ CA switching further confirmed the remarkable pH responsiveness of the superwetting surface.

To demonstrate the applicability of the POCT platform in a broad population, we investigated the surface wettability under different interfering environments. As shown in Fig. 2h, the CA remained nearly constant despite the distinct color of the droplets (pH 7), which indicated the suitability of the method for people with color blindness or color weakness. Unlike with optical detection, hundreds of millions of people, especially those with color blindness or color weakness, are expected to be included as potential customers. Furthermore, we can store the superwetting surfaces in daily ambient environments with temperatures varying from 4 to 55 °C. As expected, such temperature variations barely affected the CA (Figure S6). In addition, even when the working pressure decreased to 0.5 atm, the superwetting surface still exhibited satisfactory performance (CA = 151.2° ± 1.8°), which means it can be used over 5000 m above sea level. Unlike the pressure-based method³⁹, the CA-based method is suitable for application in all countries.

Surface tension might be a factor that affects the CA. Hence, the surface tensions of solutions with different pH values were tested (Figure S7). It can be seen that surface

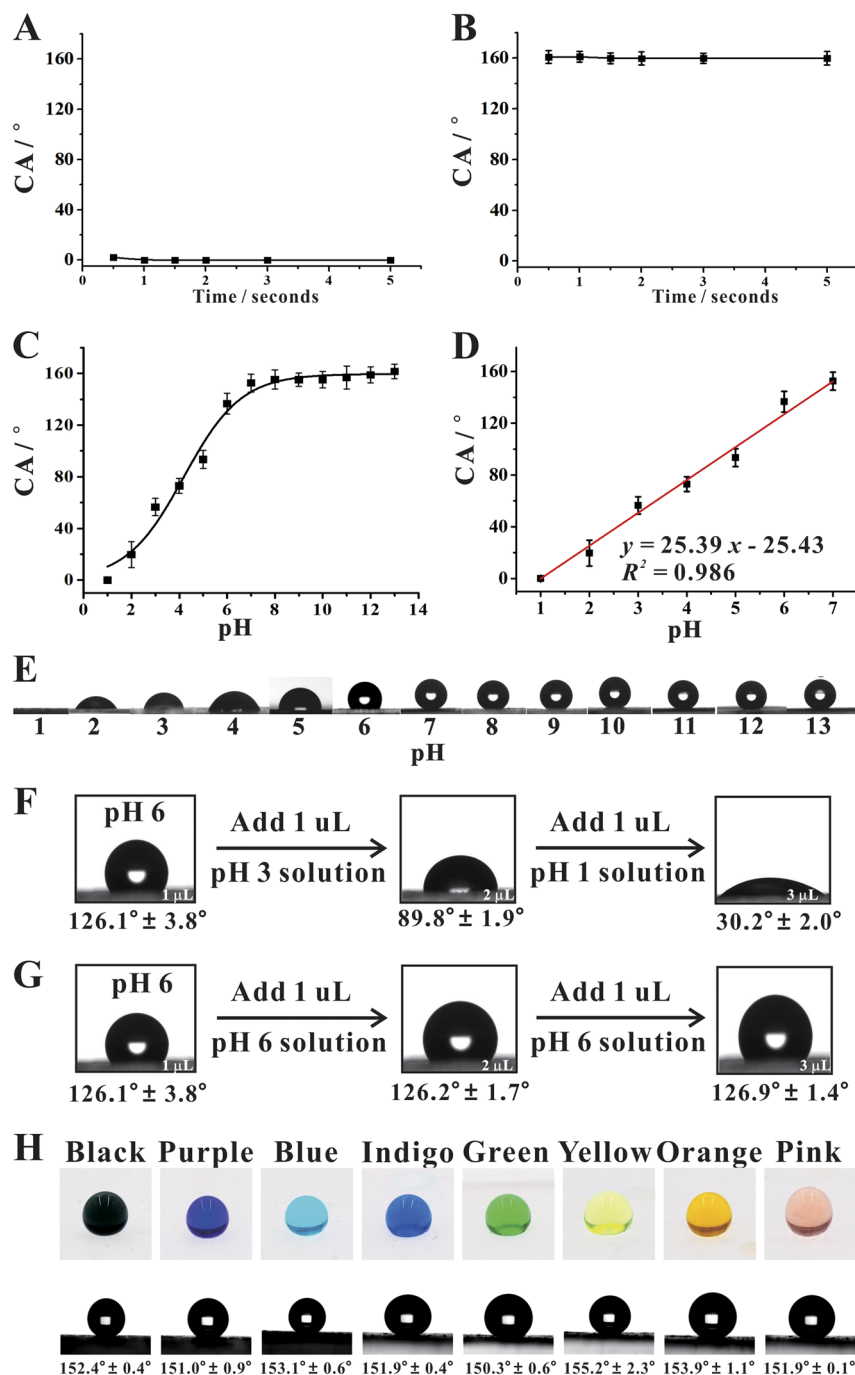


Fig. 2 **a** Relationship between the CA and the wetting time in the presence of an acidic solution (pH 1). **b** Relationship between the CA and the wetting time in the presence of an alkaline solution (pH 13). **c** Calibration curve over a wide range from pH 1 to 13 examining the relationship between the CA and pH. **d** Linear relationship between the CA and pH from 1 to 7. **e** Wetting states of droplets with different pH values. The volume of the test droplet is 2 μ L. **f** Wetting states of in situ neutralization of the superwetting surface by mixing 1 μ L of a pH 6 solution with 1 μ L of pH 3 and 1 μ L of pH 1 solutions sequentially. **g** Control experiment of in situ neutralization using a pH 6 solution instead of pH 3 and pH 1 solutions. Error bars indicate the standard deviation of three replicates. **h** Digital photos and CA measurements of droplets with distinct colors

tension was nearly constant (approximately 71.8 mN/m) for different pH values ranging from 1 to 13. As the surface tension of water is 71.8 mN/m at 20 °C, the change

in the pH barely influenced the surface tension of the solution. Thus, the surface tension is not a key factor and has a negligible effect on the CA switching in this system.

The super wettability of the as-prepared superwetting surface was found to be maintained even after at least 10 cycles with pH 1 and 13 solutions (Figure S8). The super wettability could be recovered by rinsing the surface with absolute ethanol before drying at 80 °C. Whenever the basic solution was tested, the rinsing step was not necessary because of the self-cleaning property of the superhydrophobic surface. The regenerated pH-responsive superwetting surface can avoid the fatal weakness of irreproducibility and enhance the reliability of the detection.

To evaluate the biosensing performance of the pH-responsive superwetting surface, we chose urea as a model molecule for detection. Urea can be hydrolyzed into ammonium and hydroxyl ions (OH⁻) based on the urease-catalyzed reaction to raise the pH of the solution⁴⁰. The generated OH⁻ ions caused a switch in the properties of the superwetting surface from hydrophilic to hydrophobic (Fig. 3a). We analyzed urea over a wide range of concentrations from 100 nM to 3 mM (Fig. 3b). It was noted that the CA increased with increasing urea concentration. The linear response occurred in the range from 100 nM to 1 μM (Fig. 3c). The CA was nearly constant at urea concentrations above 1 mM. By analyzing and fitting the resultant data, the linear equation $y = 44.39x + 55.61$ was obtained with a correlation coefficient of 0.993. A detection limit of 29 nM was obtained based on $S/N = 3$. Figure 3d illustrates visual images of the CA with different urea concentrations, indicating that the urea can be detected by the naked eye based on the change in the CA.

To examine the selectivity for urea detection, the effects of interfering agents, such as Na⁺, K⁺, ascorbic acid, glucose, and glycine, were investigated by comparing the CAs (Fig. 3e). In this experiment, all agents were used as 1 mM solutions for the urease-catalyzed reaction. It was observed that the CA slightly changed with the addition of interfering agents. Conversely, a significant change in the CA was obtained when 1 mM urea was added to the system. Thus, it was proposed that these interferences barely influence urea detection because of the remarkable specificity of the urease-catalyzed reaction to urea.

To demonstrate that the pH-responsive superwetting surface is applicable to the detection of other biomolecules, we examined the glucose detection ability, as shown in Fig. 4a. In the glucose detection method, a glucose oxidase (GOx)-catalyzed reaction in which glucose was converted to gluconic acid, providing free hydrogen ions (H⁺), was employed^{41,42}. The generated protons reduced the pH of the solution, resulting in a decrease in the CA. Based on the switching of the wetting property, we can establish a sensing strategy for the naked-eye detection of glucose using CA as the readout signal.

A series of experiments were performed to optimize the conditions for glucose detection. First, we investigated the GOx-catalyzed reaction with different reaction times (0–120 min). It was recognized that the CA gradually decreased with increasing reaction time. After 40 min of incubation, the CA decreased significantly and then remained nearly constant (Figure S9A). Subsequently, the concentration of GOx was optimized. We found that the CA decreased with increasing GOx concentration (Figure S9B). The CA achieved a plateau at a GOx concentration of 6 U mL⁻¹, and after that, the CA remained nearly stable even when the GOx concentration was further increased.

To examine the sensitivity of our superwetting surface in glucose detection, GOx-catalyzed reactions activated by glucose were carried out over a wide range of glucose concentrations from 1 nM to 1 mM (Fig. 4b). It can be seen that the CA linearly decreased with increasing concentration in the range from 1 to 800 nM (Fig. 4c). By analyzing and fitting the resultant data, it was found that the linear correlation coefficient of this range is 0.988 with a linear equation of $y = -48.70x + 130.6$ and a detection limit of 0.32 nM ($S/N = 3$). Figure 4d shows visual images of glucose solution droplets from 1 to 800 nM on the superwetting surface, indicating that glucose can be detected by the naked eye based on the change in the CA.

The CAs of solutions with and without glucose have been studied theoretically and experimentally (Fig. 4e). Since 1.0 μmol of glucose can be oxidized to gluconic acid and H₂O₂ by 1 U of GOx per min⁴³, 4.8×10^{-5} M protons can be theoretically produced after 60 min of incubation when 0.8 μM glucose and 10 U mL⁻¹ GOx are added. The theoretical pH ($\text{pH} = -\lg [\text{H}^+]$) would then be 4.3. Based on the pH-responsive curve ($y = 25.39x - 25.43$, where x is the pH and y is the CA.), the theoretical CA would be 83.7°, which is close to the experimental CA (90.3°). Considering that the reaction efficiency is not exactly 100%, it is reasonable that the experimental CAs are generally higher than the theoretical CAs when different concentrations of glucose are examined. The irregular gap between the experimental and theoretical CAs might result from multiple factors. For instance, the temperature and humidity might have influences on the output CA¹, the generated acid could affect the activity of GOx⁴³, and the buffer resistance might be another impact factor^{26,27}.

To evaluate the selectivity of our assay, other monosaccharide substances, such as fructose, galactose, mannose, arabinose, and xylose, were used as interfering agents. As shown in Fig. 4f, the CA changed remarkably in the presence of glucose. Of note, slight changes in the CA were found when other interfering agents were added to the system. This result might be attributed to the fact that GOx reacted specifically with β-D-glucose and barely reacted with the other analogs.

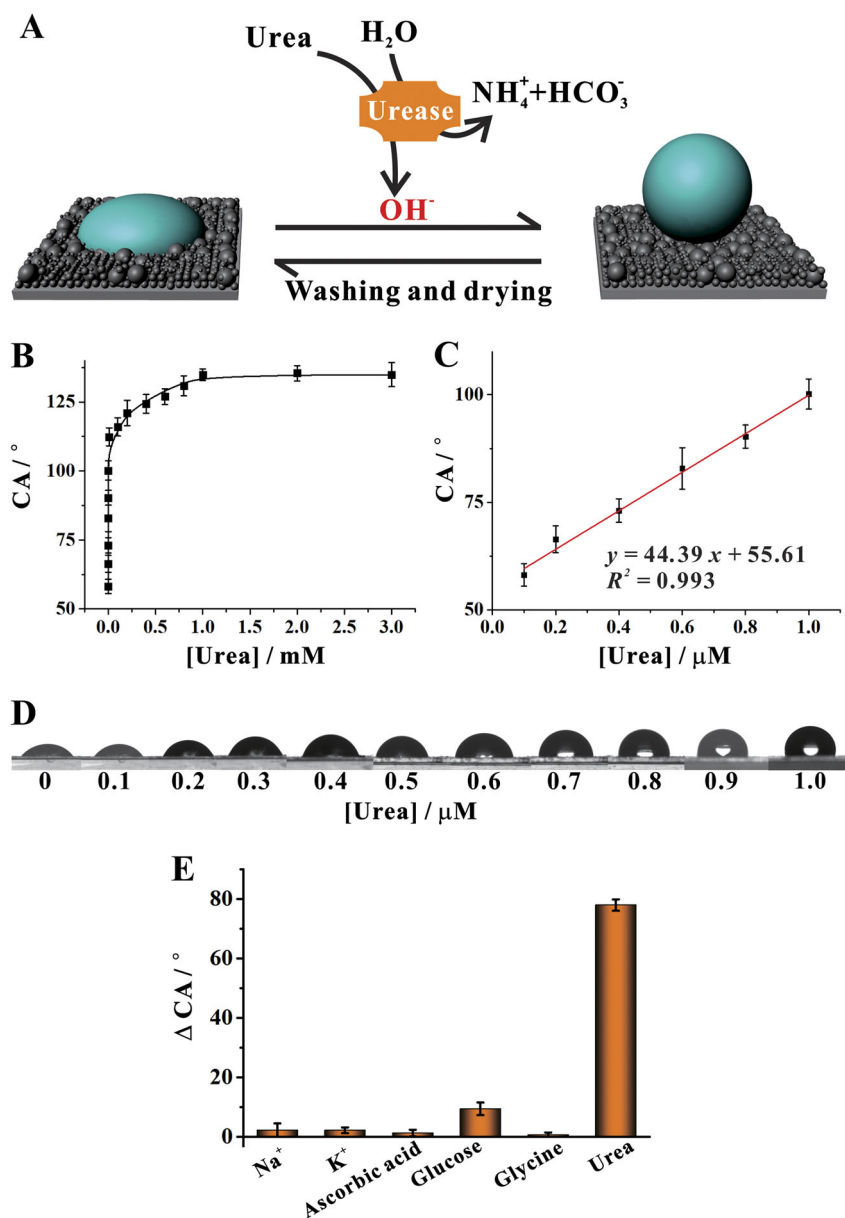


Fig. 3 Illustration of urea detection by the pH-responsive superwetting surface. **a** Schematic representation of urea detection based on the OH⁻ released from the urease-catalyzed reaction. The surface could be reused after washing and drying. **(b)** Sensitivity test with different concentrations of urea (100, 200, 400, 600, 800 nM and 1, 10, 100, 200, 400, 600, 800, 1, 2, and 3 mM). **c** Linear relationship between the CA and urea concentrations ranging from 100 nM to 1 μM. **d** Wetting states of droplets with different concentrations of urea within the linear range. **e** Relationship between the change in the CA ($\Delta CA = |CA - CA_0|$, where CA and CA₀ are the CAs of the experimental group and the blank control, respectively) and interfering agents (Na⁺, K⁺, ascorbic acid, glucose, and glycine). All substances were tested at 1 mM with 10 U mL⁻¹ of urease at 37 °C for 10 min of incubation. The initial pH was 3. The volume of the test droplet was 2 μL. Error bars refer to the standard deviation of three replicates

Taken together, our results reveal that a POCT platform has been established for the naked-eye detection of various targets, including the pH, urea, and glucose, based on the pH-responsive superwetting surface.

To evaluate the practicability and confirm the accuracy of the POCT platform, we chose glucose for invasive and

noninvasive disease biomarker detection since diabetes mellitus continues to be a major burden on society globally. In glucose detection, biofluids, such as blood, urine, saliva, and sweat, might be used as biomarkers for clinical monitoring of diabetes⁴⁴. The normal glucose concentrations in biofluids are 4–8 mM in blood⁴⁵,

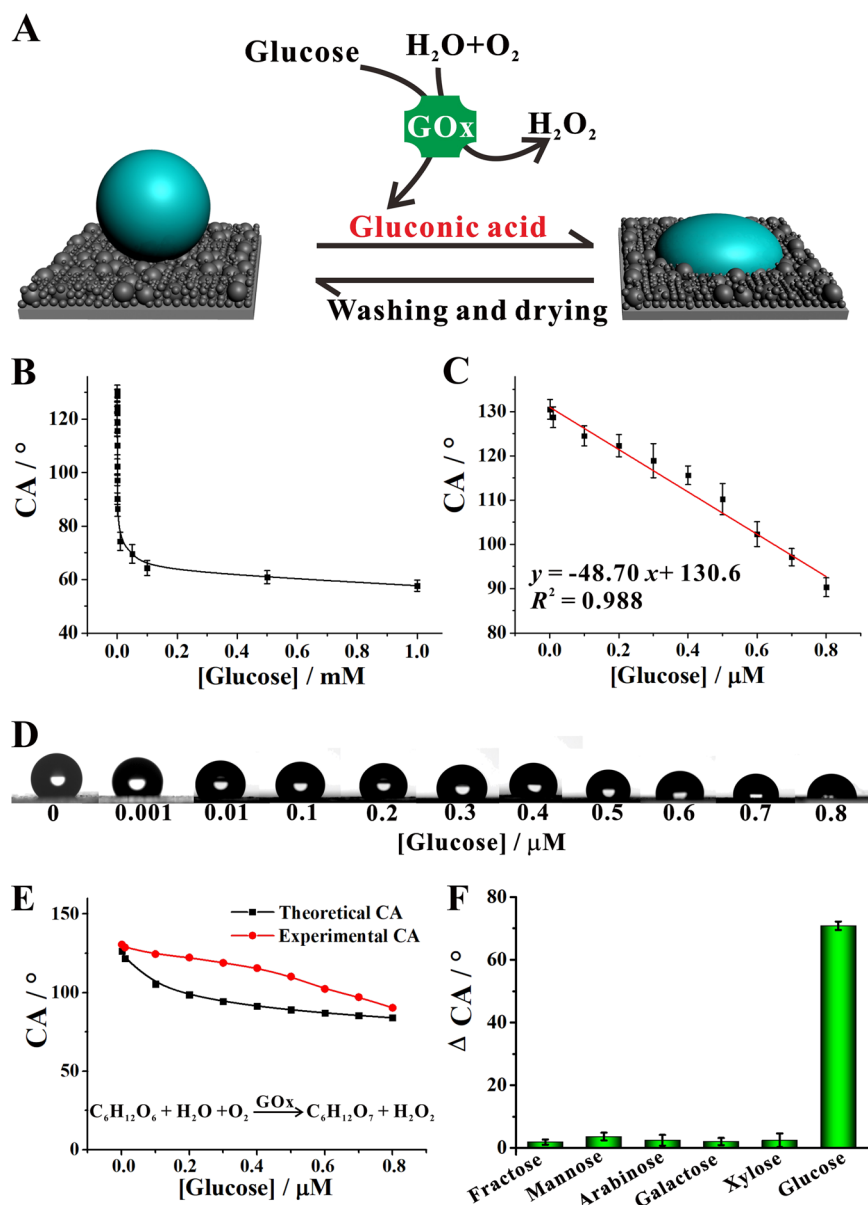
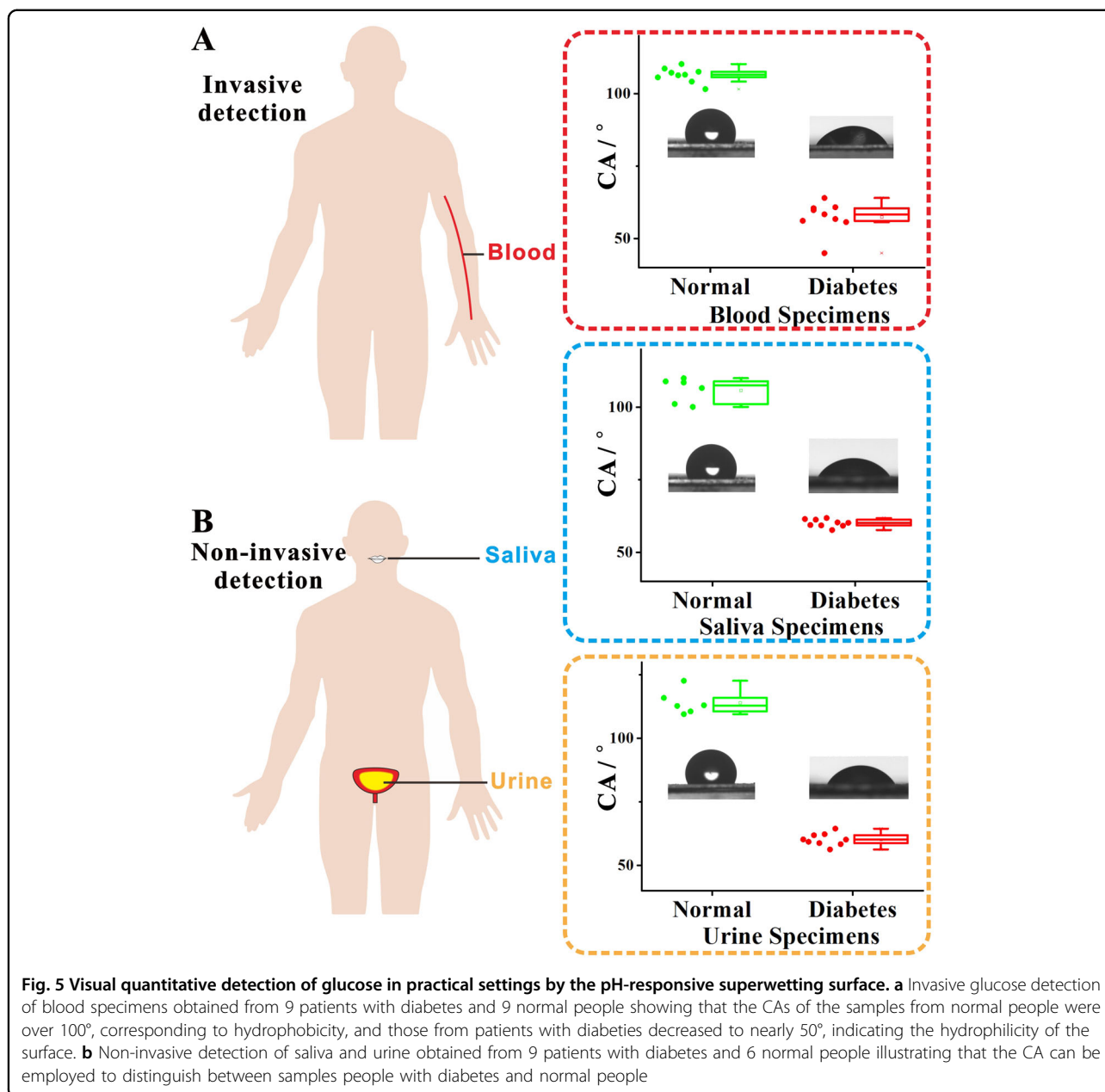


Fig. 4 Illustration of glucose detection by the pH-responsive superwetting surface. **a** Schematic representation of glucose detection based on the gluconic acid released from the GOx-catalyzed reaction. The surface could be reused after washing and drying. **b** Sensitivity test with different concentrations of glucose (1, 10, 100, 200, 300, 400, 500, 600, 700, 800 nM and 1, 10, 50, and 100 μM , 500 μM and 1 mM). **c** Linear relationship between the CA and glucose concentrations ranging from 1 nM to 800 nM. **d** Wetting states of droplets with different concentrations of glucose within the linear range. **e** The theoretical and experimental CA in the presence of different glucose concentrations ranging from 1 nM to 800 nM. The theoretical CA was obtained from the pH-responsive curve. **f** Relationship between the change in the CA ($\Delta\text{CA} = |\text{CA} - \text{CA}_0|$, where CA and CA_0 are the CAs of the experimental group and the blank control, respectively) and interfering agents (fructose, mannose, arabinose, galactose, xylose and glucose). The interfering substances were tested at 0.5 mM with 10 U mL⁻¹ GOx at 37 °C for 60 min of incubation. The initial pH was 6. The volume of the test droplet was 2 μL . Error bars indicate the standard deviation of three replicates

0.5–2.8 mM in urine⁴⁶, 0.008–0.21 mM in saliva⁴⁵ and 0.005–1 mM in sweat, which is correlated with the blood glucose concentration⁴⁴. Glucose homeostasis refers to the maintenance of a stable glucose level within the body by the balancing of insulin and glucagon. However, in a disturbed glucose homeostasis, insulin resistance and

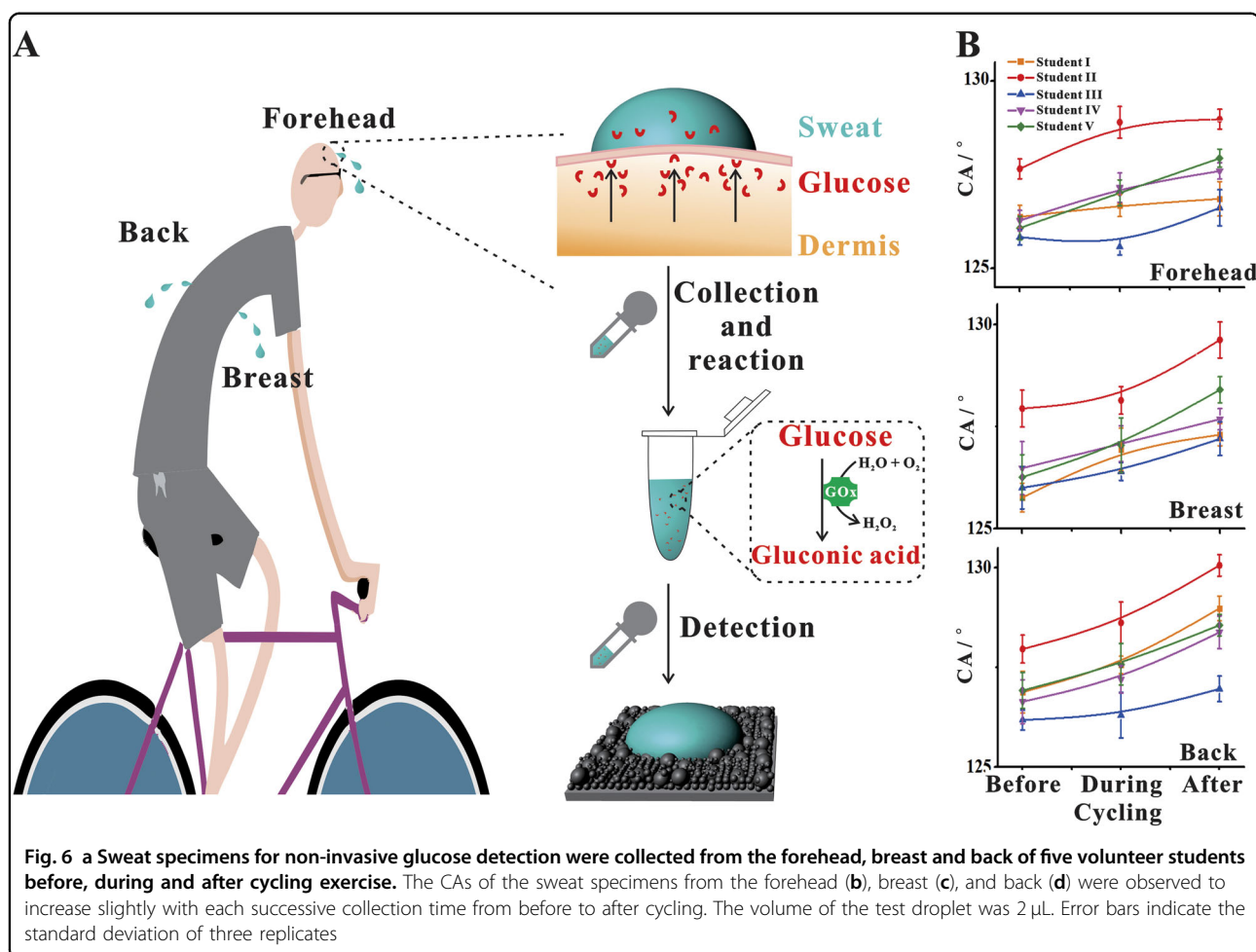
glucose intolerance produces a state characterized by the inability to maintain stable glucose levels because insulin lowers the blood glucose concentration by promoting glucose uptake⁴⁷. The control of glucose homeostasis during exercise is dictated by complex interactions between multiple hormonal regulators (e.g., insulin and



glucagon), the nervous system, and various molecular regulators within skeletal muscle and the liver, allowing for precise control of the glucose concentration during most activities⁴⁸.

Thus, our proposed POCT sensor based on CA readouts was applied to glucose detection in various fluids (blood, urine and saliva) from patients and normal people. The quantitative visual detection method was evaluated by comparing the results of the visual CA method with the results acquired by commercial glucometers. We tested a series of blood samples (diluted 1000 times before use) from 9 patients with diabetes and 9 normal people. Figure 5a indicates that the CA of all

normal specimens exhibited significantly higher values due to the apparent hydrophobicity, whereas the CAs of the samples from patients with diabetes decreased due to the hydrophilic property. According to this survey, the POCT platform is capable of distinguishing between people with diabetes and normal people by visually reading the wettability, in which relative hydrophobicity corresponds to normal blood and relative hydrophilicity indicates the occurrence of diabetes. In addition, the low relative standard deviation of this method compared with that of the commercial glucometers indicates the remarkable accuracy and reliability for real sample analysis (Table S1).



Currently, most of the commercially available glucometers are capable of tracking an individual's glucose level in the blood, which is an invasive detection method, causing pain and bringing the risk of infections, such as AIDS, hepatitis B, hepatitis C, and syphilis, to the user. Measurements of human saliva, urine, and sweat could enable facile non-invasive detection, efficiently avoiding these drawbacks due to the abundant information of glucose contained in these fluids that can be retrieved non-invasively. Figure 5b displays the non-invasive detection results for urine (diluted 250 times before use) and saliva (diluted 5 times before use) samples from 9 patients with diabetes and 6 normal people. A very low value was observed for the patient samples, whereas the CA was relatively high for the normal samples (Table S2).

Meanwhile, since the major physiological stimulators of muscle glucose uptake are exercise and insulin and because the measurement of glucose in sweat provides a potential solution for the estimation of blood glucose levels, we performed a survey of sweat glucose detection. Sweat samples from different body parts, including the forehead, breast, and back, were collected from five

pre-prandial healthy volunteers during cycling on an ergometer (Fig. 6a). We found that during cycling, the CAs of the sweat specimens (diluted 5 times before use) gradually increased for each of the different body parts, including the forehead (Fig. 6b), breast (Fig. 6c), and back (Fig. 6d). This increase in the CA implied a decrease in the glucose concentration in sweat during cycling because the glycogen that is made from glucose was consumed through exercise, which is in accordance with the reported phenomenon⁴⁹. From an individual perspective, the CA followed a similar increasing trend in the analysis of the sweat from different body parts (Figure S10). Because the sweat rate or metabolic capacity of the organs varies between body parts^{49,50}, the concentration of glucose could change depending on the region where the sweat was collected. The detailed results of non-invasive glucose detection in sweat before, during, and after the cycling exercise are summarized in Table S3.

Of note, the blood, urine, saliva, and sweat specimens were diluted before the GOx-catalyzed reaction to adjust the glucose concentration into the linear range. In this case, the pH of these specimens was approximately 7.4,

which excluded interference by the inherent pH of the specimens.

Taken together, we demonstrated that the proposed POCT platform exhibits excellent performance in non-invasive glucose detection in human urine, saliva and sweat samples.

Conclusion

We have designed a rapid pH-responsive superwetting surface with superior superwettability as a POCT platform for the naked-eye determination of the pH, urea, and glucose. This surface was demonstrated to switch between being superhydrophilic and superhydrophobic properties as a function of the pH. Compared with commercial glucometers, the proposed POCT platform exhibited superior accuracy in the determination of samples from patients with diabetes. Moreover, the non-invasive diagnoses of diabetes in urine and saliva were achieved. The developed method provided a non-invasive means for monitoring changes in glucose levels during exercise. The CA-based superwettable POCT platform provided advantages of being rapid, straightforward, equipment-free, and low-cost. More importantly, the performance was barely influenced by the temperature, elevation, and color of the droplet, making it suitable for people with color blindness or color weakness and extending its applicability to hundreds of millions of people. For the nature-inspired superwettable system, this rapid-response disposable POCT sensor might overcome the limitations of the mechanical stability and durability of superwettable materials and thus extend the industrial-scale application of bioinspired superwettable systems. While the practical results gathered in this system are preliminary in scope, future studies will aim to construct detailed on-body biosensors that integrate the superwetting surface with photoelectric properties, data processing, and wireless transmission to monitor more clinically relevant sweat metabolites. We expect that the concept can be expanded to additional applications in athletic performance assessment as well as in the general healthcare field.

Acknowledgements

This work was supported by the National Basic Research Program of China (973 Program, 2015CB932600), the National Key R&D Program of China (2017YFA0208000, 2016YFF0100800), the National Natural Science Foundation of China (21525523, 21722507, 21574048, 21605053), The Fok Ying-Tong Education Foundation, China (151011) and the China Postdoctoral Science Foundation (2016M602276).

Author details

¹Hubei Key Laboratory of Bioinorganic Chemistry & Materia Medica, School of Chemistry and Chemical Engineering, Department of Obstetrics and Gynecology, Tongji Hospital, Tongji Medical College, Huazhong University of Science and Technology, 430074 Wuhan, China. ²Engineering Research Center of Nano-Geomaterials of Ministry of Education, Faculty of Materials Science and Chemistry, China University of Geosciences, 388 Lumo Road, 430074 Wuhan, China. ³Institute of Molecular Medicine, Shanghai Jiao Tong University, 200240 Shanghai, China. ⁴Key Laboratory of Bio-Inspired Smart Interfacial

Science and Technology of Ministry of Education, School of Chemistry, Beihang University, 100191 Beijing, China

Conflict of interest

The authors declare that they have no conflict of interest.

Publisher's note

Springer Nature remains neutral with regard to jurisdictional claims in published maps and institutional affiliations.

Supplementary information is available for this paper at <https://doi.org/10.1038/s41427-018-0024-7>.

Received: 19 November 2017 Revised: 20 December 2017 Accepted: 30 December 2017.

Published online: 11 April 2018

References

- Liu, M., Wang, S. & Jiang, L. Nature-inspired superwettability systems. *Nat. Rev. Mater.* **2**, 17036 (2017).
- Cape, J. N. Contact angles of water droplets on needles of Scots pine (*Pinus sylvestris*) growing in polluted atmospheres. *New Phytol.* **93**, 293–299 (1983).
- Percy, K. E. & Baker, E. A. Effects of simulated acid rain on leaf wettability, rain retention and uptake of some inorganic ions. *New Phytol.* **108**, 75–82 (1988).
- Nagase, K. et al. Effects of graft densities and chain lengths on separation of bioactive compounds by nanolayered thermoresponsive polymer brush surfaces. *Langmuir* **24**, 511–517 (2008).
- Kahn, J. S., Hu, Y. & Willner, I. Stimuli-responsive DNA-based hydrogels: from basic principles to applications. *Acc. Chem. Res.* **50**, 680–690 (2017).
- Lu, Y., Aimetti, A. A., Langer, R. & Gu, Z. Bioresponsive materials. *Nat. Rev. Mater.* **1**, 16075 (2016).
- Zhang, W. et al. Microfluidics separation reveals the stem-cell-like deformability of tumor-initiating cells. *Proc. Natl Acad. Sci.* **109**, 18707–18712 (2012).
- Zhou, J., Lu, X., Hu, J. & Li, J. Reversible immobilization and direct electron transfer of cytochrome c on pH sensitive polymer interface. *Chem. Eur. J.* **13**, 2847–2853 (2007).
- Zhou, J., Wang, G., Hu, J., Lu, X. & Li, J. Temperature, ionic strength and pH induced electrochemical switch of smart polymer interfaces. *Chem. Commun.* **0**, 4820–4822 (2006).
- Stuart, M. A. C. et al. Emerging applications of stimuli-responsive polymer materials. *Nat. Mater.* **9**, 101–113 (2010).
- Verho, T. et al. Reversible switching between superhydrophobic states on a hierarchically structured surface. *Proc. Natl Acad. Sci.* **109**, 10210–10213 (2012).
- Lafuma, A. & Quéré, D. Superhydrophobic states. *Nat. Mater.* **2**, 457–460 (2003).
- Krumpfer, J. W. & McCarthy, T. J. Dip-coating crystallization on a superhydrophobic surface: a million mounted crystals in a 1 cm² array. *J. Am. Chem. Soc.* **133**, 5764–5766 (2011).
- Cheng, M. et al. Bell-shaped superhydrophilic—superhydrophobic—superhydrophilic double transformation on a pH-responsive smart surface. *Adv. Mater.* **26**, 306–310 (2014).
- Ganesh, V. A., Raut, H. K., Nair, A. S. & Ramakrishna, S. A review on self-cleaning coatings. *J. Mater. Chem.* **21**, 16304 (2011).
- Kreder, M. J., Alvarenga, J., Kim, P. & Aizenberg, J. Design of anti-icing surfaces: smooth, textured or slippery? *Nat. Rev. Mater.* **1**, 15003 (2016).
- Pinchasik, B. E., Kappel, M. & Butt, H. J. Small structures, big droplets: the role of nanoscience in fog harvesting. *ACS Nano* **10**, 10627–10630 (2016).
- Tian, D., Song, Y. & Jiang, L. Patterning of controllable surface wettability for printing techniques. *Chem. Soc. Rev.* **42**, 5184 (2013).
- Wang, B., Liang, W., Guo, Z. & Liu, W. Biomimetic super-lyophobic and super-lyophilic materials applied for oil/water separation: a new strategy beyond nature. *Chem. Soc. Rev.* **44**, 336–361 (2015).
- Huang, X., Liu, Y., Yung, B., Xiong, Y. & Chen, X. Nanotechnology-enhanced no-wash biosensors for in vitro diagnostics of cancer. *ACS Nano* **11**, 5238–5292 (2017).
- Martinez, A. W., Phillips, S. T., Butte, M. J. & Whitesides, G. M. Patterned paper as a platform for inexpensive, low-volume, portable. *Angew. Chem. Int. Ed.* **46**, 1318–1320 (2010).

22. Liu, M. et al. Target-induced and equipment-free DNA amplification with a simple paper device. *Angew. Chem. Int. Ed.* **55**, 2709–2713 (2016).
23. Elghariani, R. Selective colorimetric detection of polynucleotides based on the distance-dependent optical properties of gold nanoparticles. *Science* **277**, 1078–1081 (1997).
24. Chapman, R. et al. Multivalent nanoparticle networks enable point-of-care detection of human phospholipase-A2 in serum. *ACS Nano* **9**, 2565–2573 (2015).
25. Pardee, K. et al. Paper-based synthetic gene networks. *Cell* **159**, 940–954 (2014).
26. Hsieh, K., Ferguson, B. S., Eisenstein, M., Plaxco, K. W. & Soh, H. T. Integrated electrochemical microsystems for genetic detection of pathogens at the point of care. *Acc. Chem. Res.* **48**, 911–920 (2015).
27. Labib, M., Sargent, E. H. & Kelley, S. O. Electrochemical methods for the analysis of clinically relevant biomolecules. *Chem. Rev.* **116**, 9001–9090 (2016).
28. Zheng, G., Patolsky, F., Cui, Y., Wang, W. U. & Lieber, C. M. Multiplexed electrical detection of cancer markers with nanowire sensor arrays. *Nat. Biotechnol.* **23**, 1294–1301 (2005).
29. Imani, S. et al. Wearable chemical–electrophysiological hybrid biosensing system for real-time health and fitness monitoring. *Nat. Commun.* **7**, 11650 (2016).
30. Zhu, Z. et al. Translating molecular recognition into a pressure signal to enable rapid, sensitive, and portable biomedical analysis. *Angew. Chem. Int. Ed.* **54**, 10448–10453 (2015).
31. Xiang, Y. & Lu, Y. Using personal glucose meters and functional DNA sensors to quantify a variety of analytical targets. *Nat. Chem.* **3**, 697–703 (2011).
32. Chen, Y. et al. Double-enzymes-mediated bioluminescent sensor for quantitative and ultrasensitive point-of-care testing. *Anal. Chem.* **89**, 5422–5427 (2017).
33. Wei, Q. et al. Detection and spatial mapping of mercury contamination in water samples using a smart-phone. *ACS Nano* **8**, 1121–1129 (2014).
34. Wong, B. Color blindness. *Nat. Methods* **8**, 441–441 (2011).
35. Lin, L., Yan, J. & Li, J. Small-molecule triggered cascade enzymatic catalysis in hour-glass shaped nanochannel reactor for glucose monitoring. *Anal. Chem.* **86**, 10546–10551 (2014).
36. Wen, Z., Ci, S. & Li, J. Pt nanoparticles inserting in carbon nanotubes arrays nanocomposites for glucose biosensors. *J. Phys. Chem. C* **113**, 13482–13487 (2009).
37. Deng, X., Mammen, L., Butt, H. J. & Vollmer, D. Candle soot as a template for a transparent robust superamphiphobic coating. *Science* **335**, 67–70 (2012).
38. Tuteja, A. et al. Designing superoleophobic surfaces. *Science* **318**, 1618–1622 (2007).
39. Huang, J., Cheng, F., Binks, B. P. & Yang, H. PH-responsive gas-water-solid interface for multiphase catalysis. *J. Am. Chem. Soc.* **137**, 15015–15025 (2015).
40. Grosso, E. D., Dallaire, A. M., Vallée-Bélisle, A. & Ricci, F. Enzyme-operated DNA-based nanodevices. *Nano Lett.* **15**, 8407–8411 (2015).
41. You, M. et al. Photon-regulated DNA-enzymatic nanostructures by molecular assembly. *ACS Nano* **5**, 10090–10095 (2011).
42. Liu, B., Sun, Z., Huang, P. J. J. & Liu, J. Hydrogen peroxide displacing DNA from nanocerium: Mechanism and detection of glucose in serum. *J. Am. Chem. Soc.* **137**, 1290–1295 (2015).
43. Nakamura, B. S. & Ogura, Y. Action mechanism of glucose oxidase of *Aspergillus niger*. *J. Biochem.* **63**, 308–316 (1968).
44. Lee, H. et al. Wearable/disposable sweat-based glucose monitoring device with multistage transdermal drug delivery module. *Sci. Adv.* **3**, 1–9 (2017).
45. Liu, C. et al. A glucose oxidase-coupled DNAzyme sensor for glucose detection in tears and saliva. *Biosens. Bioelectron.* **70**, 455–461 (2015).
46. Zhang, Z., Chen, Z., Cheng, F., Zhang, Y. & Chen, L. Highly sensitive on-site detection of glucose in human urine with naked eye based on enzymatic-like reaction mediated etching of gold nanorods. *Biosens. Bioelectron.* **89**, 932–936 (2017).
47. Ruud, J., Steculorum, S. M. & Bru, J. C. Neuronal control of peripheral insulin sensitivity and glucose metabolism. *Nat. Commun.* **8**, 15259 (2017).
48. Riddell, M. & Perkins, B. A. Exercise and glucose metabolism in persons with diabetes mellitus: Perspectives on the role for continuous glucose monitoring. *J. Diabetes Sci. Technol.* **3**, 914–923 (2009).
49. Gao, W. et al. Fully integrated wearable sensor arrays for multiplexed in situ perspiration analysis. *Nature* **529**, 509–514 (2016).
50. Sonner, Z. et al. The microfluidics of the eccrine sweat gland, including biomarker partitioning, transport, and biosensing implications. *Biomechanics* **9**, 031301 (2015).